Microscopic origin of granular fluidity: An experimental investigation

Rebecca N. Poon [1,2,*] Amalia L. Thomas [3,1] and Nathalie M. Vriend [5,1,4,3]

[1] *BP Institute, University of Cambridge, Madingley Rise, Madingley Road, Cambridge CB3 0EZ, United Kingdom*

[2] *Living Systems Institute, University of Exeter, Stocker Road, Exeter, EX4 4QD, United Kingdom*[†]

[3] *Department of Applied Mathematics & Theoretical Physics, University of Cambridge, Centre for Mathematical Sciences, Wilberforce Road, Cambridge CB3 0WA, United Kingdom*

[4] *Department of Earth Sciences, University of Cambridge, Downing Street, Cambridge CB2 3EQ, United Kingdom*

[5] *Paul M. Rady Department of Mechanical Engineering, University of Colorado, Boulder, 1111 Engineering Drive, Boulder, Colorado 80309, USA*[†]

(Received 9 May 2023; accepted 30 October 2023; published 4 December 2023)

Granular fluidity has been central to the development of nonlocal constitutive equations, which are necessary for characterizing nonlocal effects observed in experimental granular flow data. However, validation of these equations has been largely computational due to challenges in laboratory experiments. Specifically, the origin of the fluidity on a microscopic, single-particle level is still unproven. In this work, we present an experimental validation of a microscopic definition of granular fluidity, and show the importance of basal boundary conditions to the validity of the theory.

DOI: 10.1103/PhysRevE.108.064902

Granular materials are classified as a "complex fluid" [1]: a multiphase material whose flow cannot be described by a Newtonian rheology. The conventional $\mu(I)$ rheology developed by GDR-MiDi [2] and Jop *et al.* [3] has been successful in predicting many aspects of granular flows, but has significant shortcomings. Specifically, the "nonlocal phenomena" [4] that are abundant in granular observations, for example a creeping "static" granular pack and the thin layer of material left behind after an avalanche, cannot be replicated with a local rheological model. In order to correctly describe these nonlocal manifestations, it is not sufficient to model a linear relationship between the strain rate and stress [5]. Great advancements have been made in recent years in theoretical modeling of such nonlocal phenomena, with a variety of constitutive relations being proposed [6–8]. However, experimental validation lags behind model development due to the complexity of these experiments. In this manuscript, we present experimental findings that enable us to validate a key theoretical relationship in nonlocal granular flow theory.

To construct nonlocal constitutive equations for granular flow, Kamrin and Koval [7] extended the kinetic elastoplastic (KEP) model of Bocquet *et al.* [9]—originally formulated to describe nonlocality in emulsions—to a granular material application. In the KEP model the key additional variable is the fluidity: a phenomenologically defined parameter describing how "deformable" a system is. The fluidity vanishes for static regions and reaches a maximum value in fully fluidized regions [5].

Kamrin and Koval defined the granular fluidity g_{macro},

$$g_{\text{macro}} = \frac{\dot{\gamma}}{\mu}, \tag{1}$$

where $\dot{\gamma}$ is the shear rate, and $\mu = \tau/P$ is the ratio between the shear stress τ and pressure P. They used this fluidity to construct a set of nonlocal constitutive equations, which have successfully described nonlocal phenomena in both experiments [10] and DEM simulations [7]. The predictive success of these constitutive equations supports the importance of the fluidity in nonlocal descriptions.

However, the fluidity used in their constitutive equations is only defined in terms of macroscopic flow quantities: the definition in Eq. (1) is operational, and gives no insight into the physical origin of the fluidity on a single particle level. Thus, Zhang and Kamrin [11] (ZK) subsequently proposed a microscopic fluidity,

$$g_{\text{micro}} = \frac{\delta v}{d} F(\Phi), \tag{2}$$

where δv quantifies single-particle velocity fluctuations around the spatial mean value, d is the particle diameter, and $F(\Phi)$ is a general function of the local volume fraction Φ. Computational and theoretical studies have found $F(\Phi)$ to be constant for intermediate Φ, falling to zero as Φ approaches a critical value [11–14]. ZK validated their proposed definition by numerical simulations in three different 3D geometries. More recently, DEM simulations in other geometries have shown a partial agreement with ZK's definition [15].

Experimental validation of the equivalence of the microscopic and macroscopic expressions for fluidity in a single

*rp606@exeter.ac.uk

†Present address.

system is still limited; previous testing of the theory has been carried out largely by numerical simulations. This is partly due to the difficulty in concurrently measuring both kinematic ("velocity") and dynamic ("force") properties. The relevant quantities have been experimentally measured in some previous studies using wall-averaged measurements of the stress [16], and at very low inertial number ($I < 10^{-4}$) [17].

In this article, we provide an experimental validation of the ZK definition, using an existing experimental setup designed to create a two-dimensional avalanche of photoelastic disks, resulting in granular flows with large values of the inertial number I and allowing access to individual particle stress measurements [18]. Previously we used this setup to find a correlation between the fluidity and the fluctuation rate of force chains in the flow [19]. Here we measure and calculate the kinematic properties of our flow, and combine them with our published measurements of the dynamic flow properties, in order to experimentally validate the ZK definition outlined in Eq. (2). We use particle tracking to access the velocity fluctuations δv and the packing fraction Φ, and photoelastic analysis [18] to obtain the stress ratio μ.

The proposed equivalence of g_{macro} and g_{micro} implies the existence of a function $F(\Phi)$ that is universal for the system, where

$$F(\Phi) \equiv \frac{\dot{\gamma}}{\mu}\frac{d}{\delta v} \tag{3}$$

from Eqs. (1) and (2). The dimensionless quantity $\dot{\gamma} d/\delta v$ was introduced by Savage and Jeffrey, who showed that it should be a function of Φ [20]. The existence of this function has also been shown numerically and experimentally [16,17]. We have previously shown that μ is a function of Φ in our system for one basal boundary condition. In this letter we further calculate the kinematic quantity $\dot{\gamma} d/\delta v$, and combine it with μ to find the function $F(\Phi)$ for our system with two basal boundary conditions. We then compare our $F(\Phi)$ to those previously found by numerical [11–13] and theoretical methods [14]. This comparison requires accounting for the difference in dimensionality between our experiments and previous work: experimental constraints limit us to a 2D setup, while previous numerical simulations have been conducted for 3D systems. However, we are able to make an appropriate conversion between the 3D volume and 2D area fractions, and find a strong similarity between our empirical form and those predicted in previous studies. Lastly, we interpret the shape of $F(\Phi)$ in terms of the jamming transition in dense granular flows.

Our experimental setup has been extensively introduced by Thomas and Vriend [18], and involves 2D avalanches of photoelastic disks as illustrated in Fig. 1. We use equal numbers of disks of diameters 11, 12, and 13 mm, equivalent to a 10% polydispersity, which reduces crystallization. The material flows down a narrow 2 m long chute, inclined at 20° to the horizontal, and has a free surface as a top boundary condition, and an either smooth or roughened bottom boundary condition. We use the coordinate system shown in Fig. 1: x points in the downstream direction with its origin at the chute mouth, and z points upwards, perpendicular to the chute base. The chute is slightly wider than the thickness of a particle, leaving enough space for the particles to flow freely with

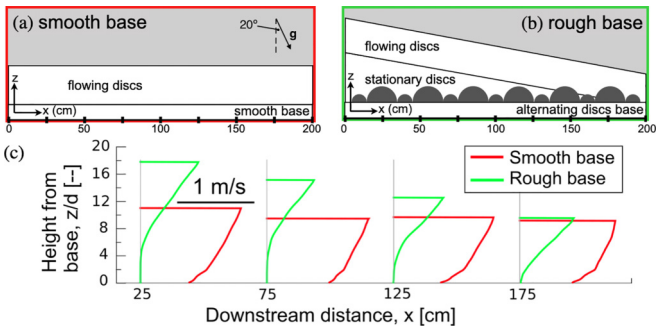

FIG. 1. Schematic of the experimental setup for different boundary conditions (a), (b) with sample velocity profiles for both (c). The chute is inclined at 20° to the horizontal, so gravity is in the direction indicated by **g**. Different basal conditions give rise to different flow profiles. The smooth base (a) has a constant flowing layer, while the rough base (b) features a wedge of quasistatic particles (on timescales 1–100 ms) that accumulate along the entire length of the base, with flowing particles above. In both bases, the height of the layer of flowing particles is approximately constant in x. Velocity profiles are taken from full data in [18].

minimal side wall friction, but not enough to rotate out of the plane of the chute, resulting in a single layer in the lateral direction. A pair of polarizer sheets, one on either side of the chute, are attached to a sliding carriage, allowing photoelastic visualization at any downstream position.

High resolution datasets are taken for 0.5 s at a sampling frequency of 1 kHz and are acquired at four downstream locations, spaced at 50 cm intervals between $x = 25$ cm and $x = 175$ cm inclusive. The frame size is approximately $20d \times 20d$ and there are approximately 300 particles visible in each image. Further details of the experimental setup are given in [18]. For the smooth base, 175 cm dataset, only 0.3 s of data was available due to edge effects of the avalanche.

The basal boundary condition qualitatively affects the velocity profile and the flow features. A smooth perspex surface allows significant slip at the base, with an increasing x velocity as z increases, Fig. 1(a). In contrast, for a rough boundary condition, constructed from half-cut particles glued to the bottom, a quasistatic basal wedge forms, above which particles flow in a layer of constant height, Fig. 1(b). Particles at the bottom of the quasistatic wedge are stationary on timescales from 1 ms to 100 ms, but creep at longer time scales [21]. Velocity profiles of the flow are show in Fig. 1(c).

We are interested in the steady state of the avalanche, where the flow height and velocity profile are constant in time, so we let the front pass before acquiring steady state data from the main body of the avalanche. For the flowing particles (all of the smooth base data and the top layer of the rough base data), the measured flow quantities (e.g., velocity and volume fraction) are constant in x. However, the thickness of the quasistatic basal wedge in the rough base experiments varies slowly in x. It varies by $\pm 0.5d$ within each dataset and by approximately $2d$ between datasets at successive chute locations, so we average in x over the frame width of one dataset, but not over datasets at different locations.

Particle identification and tracking is performed as described in [18]. The particle radii found by this automated process are rescaled to give an average particle radius equal

to the known true value. The bulk stress tensor components P and τ are also calculated as in [18].

Particle velocities are calculated from the positions, then these individual particle quantities are used to calculate δv, Φ, and $\dot{\gamma}$ as a function of depth z for each dataset. These flow profiles are calculated instantaneously before being time averaged, since we are interested in *spatial* fluctuations as a means of understanding spatial non-locality [11]. We then coarse-grain in z as in [11], using identical coarse-graining parameters. The shear rate $\dot{\gamma} = \frac{\mathrm{d}v_x}{\mathrm{d}z}$ is calculated from the coarse-grained velocity $v_x(z)$ using a second-order finite difference method. The particle diameter d is constant in z to within $\approx$2%, i.e. the particles do not segregate with depth, so we use the average diameter value throughout.

The velocity fluctuation δv is defined in [11] as the square root of the granular temperature T, which is determined for a particle i as $T_i = |\vec{v}_i - \bar{\vec{v}}(z_i)|^2$ for particle velocity $\vec{v}_i$ and average velocity $\bar{\vec{v}}(z_i)$ at the particle depth z_i. These single-particle values are coarse-grained as in [11] to give $\bar{T}(z)$, whose square root gives the velocity fluctuation profile $\delta v(z)$.

Additional steps are needed to mitigate the effects of experimental noise, since the definition of δv is such that noise is not removed by averaging or coarse-graining. Our final step is to exclude spurious points. These are found at the top and bottom of the flow, due to factors such as: coarse-graining edge effects, systematic measurement errors when μ falls below a certain value, and the function $F(\Phi)$ being undefined for basal particles within the quasi-static wedge. Details of these steps are given in the Supplemental Materials (SM) [22].

Having calculated the parameters $\dot{\gamma}(z)$, $\delta v(z)$, $\mu(z)$ and $\Phi(z)$, we can now validate the relationship between the macroscopic and microscopic definitions of the granular fluidity, Eqs. 1 and 2. This validation is achieved by finding a form of $F(\Phi)$ for our system, then using it to plot g_{micro} against g_{macro} to test their proposed equivalence. Our data below will show qualitatively different behavior depending on the bottom boundary condition.

We first present and discuss data taken with a rough base, where the particles at the base form a quasi-static wedge. Fig. 2(a) plots the ratio $F(\Phi)$ against Φ for this data. Each color indicates a different experiment (varying the downstream position), while each point in a given dataset represents a different value of the depth z.

Our experimental geometry has a pressure release boundary condition at the surface, which limits our Φ range. To interpret our $F(\Phi)$ data, we refer to the previous work by ZK (and others) showing that the shape of $F(\Phi)$ is constant below some critical Φ value, above which it falls to zero. The lack of observable downturn in our data indicates that our Φ values lie below the critical value for our system, as discussed further below. Across our available range of Φ, $F(\Phi)$ for all datasets is thus fitted by a constant value, consistent with previously found forms of $F(\Phi)$. Taking the average of all datapoints gives the constant value as $F(\Phi) = 2.12$ over our range of Φ, with a standard deviation of 0.52.

We use our $F(\Phi)$ to plot $(\delta v/d)F(\Phi)$ against $\dot{\gamma}/\mu$, Fig. 2(c). The R^2 value of our data compared to the theoretical relationship of $g_{\mathrm{micro}} = g_{\mathrm{macro}}$ is 0.80. The definition in Eq. (2) is thus validated by these datasets. The average value of $(|g_{\mathrm{micro}} - g_{\mathrm{macro}}|)/g_{\mathrm{macro}}$ for our data is 0.2. This is comparable to the experimental errors for both axes: the uncertainties in $\dot{\gamma}/\mu$ and $(\delta v/d)F(\Phi)$ were mainly due to μ and $F(\Phi)$, respectively, which both had an error of $\sim$20%. (Errors from [21] and spread of points in Fig. 2(a) respectively.)

We now compare our form of $F(\Phi)$ from our rough base boundary condition with previous research. Forms of $F(\Phi)$ have been found by previous authors [11,14], but only in 3D. To allow comparison with this research, we must therefore "translate" 3D volume fractions into 2D area fractions. This is nontrivial, requiring physical understanding of the form of $F(\Phi)$.

In numerical simulations of frictional spheres in a variety of flow geometries, ZK found that $F(\Phi)$ is constant at two for $\Phi \lesssim 0.58$, then falls rapidly for higher values of Φ, reaching zero at $\Phi = 0.63$, Fig. 2 in Ref. [11]. ZK note that 0.63 corresponds approximately to random close packing (Φ_{RCP}). Physically, we expect a limiting behavior of $F(\Phi)$ as $\Phi \to \Phi_{\mathrm{RCP}}$, since granular materials become "frozen" at Φ_{RCP}. Additionally, for frictional systems, jamming occurs at some $\Phi_{\mathrm{jam}} < \Phi_{\mathrm{RCP}}$, with Φ_{jam} decreasing as the interparticle friction coefficient increases. We note that ZK's "downturn" value of 0.58 is the Φ_{jam} value for monodisperse spheres with ZK's friction coefficient [24].

Berzi and Jenkins [14] explained the shape of $F(\Phi)$ using kinetic theory, for a system of frictionless spheres. They find an agreement between their theoretical prediction and two sets of numerical modeling results for the same system. Their derived $F(\Phi)$ agrees with ZK's in its shape, but differs in its numerical values. First, the downturn occurs at a higher Φ value, likely due to the absence of friction in Berzi and Jenkins [14] system, so that Φ_{jam} approaches Φ_{RCP}. DEM simulations have shown that the downturn in $F(\Phi)$ occurs at lower Φ values as the interparticle friction coefficient is increased [15], confirming this hypothesis. Second, the constant value for $F(\Phi)$ at low Φ is higher (but still of order one). The low-Φ constant depends on the coefficient of restitution e of the particles, but for ZK's significantly lower e of 0.1, Berzi and Jenkins [14] predict an even higher value of $F(\Phi = 0.5) \approx 11$. (See the SM [22] for details). We therefore deduce that the presence of friction in ZK's system renders the numerical predictions of Ref. [14] unsuitable so that we are unable to use their equations to predict the low-Φ constant for our frictional system, which has the additional difference of being in 2D. However, our similar coefficient of restitution to ZK's may be responsible for our similar low-Φ value.

Experimental measurement of $F(\Phi)$ in a 2D system by Fazelpour *et al.* [17] shows a similar shape to ZK's, but a limiting value of 0.1 at low Φ, Fig. 2(a). The reason for the order of magnitude difference between this value and those found here and by ZK is unclear, although it may be to do with the inertial numbers of the system of Fazelpour *et al.* [17] being a few orders of magnitude lower than ours.

Thus, previous numerical research in 3D has found a single form for $F(\Phi)$, whose shape can be explained by kinetic theory. The precise numerical values depend on the system parameters, but it always vanishes at Φ_{RCP}, and the downturn likely begins around Φ_{jam}. The kinetic theory argument is dimensionally independent [14,25], so we expect our 2D system to display this same form of $F(\Phi)$: constant at lower values, with a downturn at Φ_{jam} and vanishing at Φ_{RCP}.

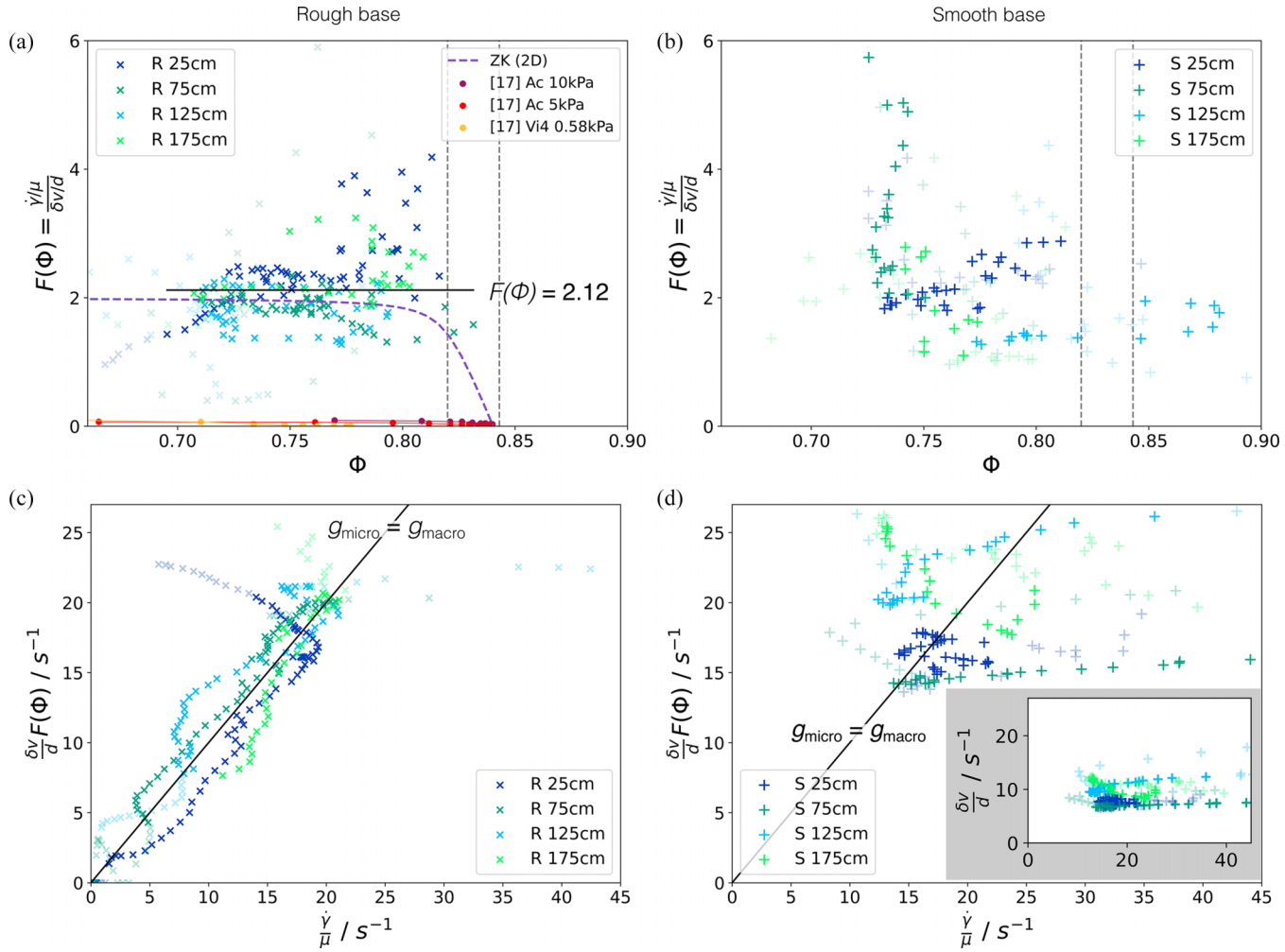

FIG. 2. (a), (b) $F(\Phi)$ for the rough and smooth bases. Dashed gray lines show 2D values for $\Phi_{\text{jam}} = 0.82$ and $\Phi_{\text{RCP}} = 0.843$ [23,24]. $F(\Phi)$ for the rough base clusters around a constant average value of 2.12 with a standard deviation of 0.52. We also plot a 2D analog of the $F(\Phi)$ predicted by ZK, with the Φ values for the downturn and vanishing points translated into a 2D system with our value of particle friction (dashed line) and plot experimental data points from another work (circle markers: see [17] for details of the experimental parameters). The smooth base is much less clustered, with a mean of 2.79 and a standard deviation of 2.10. We therefore fit $F(\Phi)$ for the rough base as a constant value of 2.12 [black line in (a)], but we do not fit $F(\Phi)$ for the smooth base. (c), (d) Correlation plots of the two fluidity definitions, Eq. (2) against (1), for the same data. Both plots use $F(\Phi) = 2.12$ from the rough base data. The black lines show the theoretical relationship, $(\delta v/d)F(\Phi) = \dot{\gamma}/\mu$. $F(\Phi)$ cannot be convincingly calculated for the smooth base, so the correlation is plotted using the $F(\Phi)$ calculated from the rough base. Although a clear correlation is no longer observed, the points loosely cluster around the theoretical prediction. The inset figure plots $\delta v/d$ against $\dot{\gamma}/\mu$ without including $F(\Phi)$. Values within $2d$ of the free surface or base, or within the quasistatic basal wedge, are plotted in fainter colors as they are affected by coarse graining and proximity to a boundary, and are therefore excluded from the analysis.

The values of Φ_{jam} and Φ_{RCP} depend on the dimensionality, polydispersity, and particle friction coefficient of the system. Φ_{RCP} for a 2D system with our polydispersity value is approximately 0.843 [26], identical to that of the commonly tested bidisperse 2D system [24]. We therefore assume that our value for Φ_{jam} is also very close to the bidisperse value at the appropriate particle friction coefficient. We use the yield stress ratio, 0.26, as the best available approximation for our particle friction coefficient [19]. By interpolation of the frictional dependence of Φ_{jam} for a bidisperse 2D system given in [24], we thus estimate our $\Phi_{\text{jam}} \approx 0.82$.

We can thus "translate" ZK's functional form of $F(\Phi)$ to our system using the relevant Φ_{jam} and Φ_{RCP}, Fig. 2(a), and see that it qualitatively compares to our data. (See the SM [22] for details.) As the majority of our Φ values are below Φ_{jam}, the absence of a significant downturn in our $F(\Phi)$ is to be expected, and we restrict ourselves to fitting a constant value for $F(\Phi)$ for our dataset, using the average value of all of the points.

We note that our boundary conditions are qualitatively different from ZK's: we have a free surface flow as opposed to their confined flow, which prevents us from accessing higher Φ values. It would be illuminating to carry out further experiments in a more confined geometry, to reach higher Φ values and ascertain whether $F(\Phi_{\text{RCP}})$ does indeed vanish for 2D frictional systems.

Although we cannot change our free surface boundary condition, we can change our basal boundary conditions. Having shown that $g_{\text{micro}} = g_{\text{macro}}$ for the rough base, we now present the smooth base data, which lacks the quasistatic basal

particles of the rough base. Figures 2(b) and 2(d) plot $F(\Phi)$ and g_{micro} against g_{macro} for this dataset. The results show clear differences to the rough base results, indicating the importance of the basal boundary condition for this theory. For the smooth base, $F(\Phi)$ is much less clustered, with a mean of 2.79 and a standard deviation of 2.10, Fig. 2(b). Thus, in contrast to the rough base data, it is not sensible to fit a single form of $F(\Phi)$. Plotting g_{micro} against g_{macro} for the smooth base, using the rough base value of $F(\Phi) = 2.12$, shows no correlation, Fig. 2(d).

We therefore conclude that the proposed microscopic fluidity definition holds in our experimental system for the rough basal boundary condition. In contrast, the relationship does not hold for the smooth basal boundary condition, indicating the importance of boundary conditions to the validity of the definition and the need for further work in this area.

Future improvements to our experimental setup could result in higher quality data. By simultaneously recording our experiments with a nonpolarizing camera, we could image the particles with improved contrast, allowing higher accuracy in our position and velocity measurements. It would also be valuable to perform experiments at higher volume fractions, to experimentally test whether $F(\Phi)$ drops as $\Phi \to \Phi_{\text{RCP}}$, as found previously [11–14,17]. Previous work using our experimental setup has found that the force chain fluctuation rate is also correlated with the fluidity [19], implying a relationship between force chain and velocity fluctuations that may be illuminating to investigate.

As the granular fluidity is key to many proposed nonlocal descriptions of granular flows, but has no widely agreed-upon definition [5], this experimental insight into its microscopic origins is a profound contribution to current research into the nature and role of fluidity in granular systems. In particular, this definition provides a link between granular fluidity and kinetic theory as approaches in nonlocal modeling of granular systems [14].

To conclude, we have found experimental evidence to support the theory that the nonlocal granular fluidity on a microscopic level is due to spatial fluctuations of the individual particle velocities. We show that the validity of the theory depends on the basal boundary condition of the flow.

We are grateful to Karen Daniels for advice and helpful discussions. We thank Jonathan Kollmer for writing, and aiding with implementing, the photoelastic force solver PeGS, which was used for the initial data processing. (Code available at [27]). We are also very thankful to technicians David Page-Croft, Paul Mitton, Colin Hitch, Andrew Denson, and John Milton for their invaluable help and technical support in the construction and maintenance of the experimental apparatus. We thank Eric Weeks for his illuminating comments on critical packing fractions of 2D systems. We thank Ben McMillan for critical reading of the manuscript. N.M.V. is supported by a Royal Society University Research Fellowship URF/R1/191332.

[1] B. Kou, J. L. Yixin Cao, C. Xia, Z. Li, H. Dong, A. Zhang, J. Zhang, W. Kob, and Y. Wang, Granular materials flow like complex fluids, Nature (London) **551**, 360 (2017).

[2] GDR-MiDi, On dense granular flows, Eur. Phys. J. E **14**, 341 (2004).

[3] P. Jop, Y. Forterre, and O. Pouliquen, Crucial role of sidewalls in granular surface flows: Consequences for the rheology, J. Fluid Mech. **541**, 167 (2005).

[4] K. Kamrin, Non-locality in granular flow: Phenomenology and modeling approaches, Front. Phys. **7**, 116 (2019).

[5] M. Bouzid, A. Izzet, M. Trulsson, E. Clément, P. Claudin, and B. Andreotti, Non-local rheology in dense granular flows, Eur. Phys. J. E **38**, 125 (2015).

[6] O. Pouliquen and Y. Forterre, A non-local rheology for dense granular flows, Phil. Trans. R. Soc. A. **367**, 5091 (2009).

[7] K. Kamrin and G. Koval, Nonlocal constitutive relation for steady granular flow, Phys. Rev. Lett. **108**, 178301 (2012).

[8] M. Bouzid, M. Trulsson, P. Claudin, E. Clément, and B. Andreotti, Nonlocal rheology of granular flows across yield conditions, Phys. Rev. Lett. **111**, 238301 (2013).

[9] L. Bocquet, A. Colin, and A. Ajdari, Kinetic theory of plastic flow in soft glassy materials, Phys. Rev. Lett. **103**, 036001 (2009).

[10] D. L. Henann and K. Kamrin, A predictive, size-dependent continuum model for dense granular flows, Proc. Natl. Acad. Sci. **110**, 6730 (2013).

[11] Q. Zhang and K. Kamrin, Microscopic description of the granular fluidity field in nonlocal flow modeling, Phys. Rev. Lett. **118**, 058001 (2017).

[12] N. Mitarai and H. Nakanishi, Velocity correlations in dense granular shear flows: Effects on energy dissipation and normal stress, Phys. Rev. E **75**, 031305 (2007).

[13] S. Chialvo and S. Sundaresan, A modified kinetic theory for frictional granular flows in dense and dilute regimes, Phys. Fluids **25**, 070603 (2013).

[14] D. Berzi and J. T. Jenkins, Fluidity, anisotropy, and velocity correlations in frictionless, collisional grain flows, Phys. Rev. Fluids **3**, 094303 (2018).

[15] J. A. Robinson, D. J. Holland, and L. Fullard, Examination of the microscopic definition for granular fluidity, Phys. Rev. Fluids **6**, 044302 (2021).

[16] R. Artoni, A. Soligo, J.-M. Paul, and P. Richard, Shear localization and wall friction in confined dense granular flows, J. Fluid Mech. **849**, 395 (2018).

[17] F. Fazelpour, Z. Tang, and K. E. Daniels, The effect of grain shape and material on the nonlocal rheology of dense granular flows, Soft Matter **18**, 1435 (2022).

[18] A. L. Thomas and N. M. Vriend, Photoelastic study of dense granular free-surface flows, Phys. Rev. E **100**, 012902 (2019).

[19] A. L. Thomas, Z. Tang, K. E. Daniels, and N. M. Vriend, Force fluctuations at the transition from quasi-static to inertial granular flow, Soft Matter **15**, 8532 (2019).

[20] S. Savage and D. Jeffrey, The stress tensor in a granular flow at high shear rates, J. Fluid Mech. **110**, 255 (1981).

[21] A. L. Thomas, Photoelastic study of dense granular free-surface flow rheology and size segregation, Ph.D. thesis, University of Cambridge, 2019.
[22] See Supplemental Material at http://link.aps.org/supplemental/10.1103/PhysRevE.108.064902 for details of data processing methods; profiles of the raw quantities; and comparative calculations of $F(\Phi)$ values in other systems.
[23] S. Meyer, C. Song, Y. Jin, K. Wang, and H. A. Makse, Jamming in two-dimensional packings, Physica A **389**, 5137 (2010).
[24] L. E. Silbert, Jamming of frictional spheres and random loose packing, Soft Matter **6**, 2918 (2010).
[25] J. T. Jenkins (private communication, 2020).
[26] E. R. Weeks (private communication, 2023).
[27] https://github.com/jekollmer/pegs.